VIP *Very Important Paper*

Special Collection

Controlled Lithium Deposition on Alq_3 Coated Substrate**

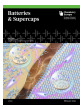

Haoxiang Zhong,[a, b] Yangzhi Zhao,[a] Ting Zhang,[c] and Gao Liu*[a]

High theoretical charge capacity (3,860 mAh g^{-1}) and low redox potential (−3.04 V vs. standard hydrogen electrode) make lithium metal a promising anode for next-generation high energy density battery. However, the practical implementation of Li-metal anode is still elusive due to poor coulombic efficiency and cycling performance as well as safety concerns caused by lithium dendrite formation and poor compatibility of liquid electrolyte with lithium. In this work, we developed a strategy to control lithium deposition and growth by using surface modified electrodes coated by a conductive chelate compound tris-(8-hydroxyquinoline) aluminum (Alq_3) onto copper current collector. As a result, Alq_3 exhibits good conductivity and electrochemical stability verified by cyclic voltammetry test. The Alq_3 can modulate lithium metal growth on Cu surface, in addition, it demonstrates morphology control of deposited lithium by tuning variables such as current density and coating thickness. Optimal cycling stability and stable coulombic efficiency over 300 cycles are observed on the Li||Alq_3/Cu cell at 50 nm coating thickness – an evidence shows controlled lithium deposition by this simple but effective surface modified electrode.

Introduction

In order to meet the zero greenhouse gas (GHG) emission target by 2050, the global vehicles, currently powered by fossil fuels, are transforming toward a new way to be powered by clean electricity. Li-ion battery plays a critical role in this transformation as it has been proven to be the most effective and mature electricity storage technology by far to sustain a vehicle for a long distance. However, the current state of the art Li-ion battery has approached the limit of theoretical energy capacity (300 Wh kg^{-1}) which falls short to meet the continued need for electric vehicles (EVs) in the future; intuitively, the increasing demand in electricity storage requires batteries with high energy density (500 Wh kg^{-1}) and low cost.[1] Over the past years, remarkable progress has been made to address this challenge by seeking new redox chemistry, developing cell configuration with advanced chemical or structural design of electrode and electrolyte materials, and developing scalable facile synthesis/manufacturing for key materials.[2–12] Notably, lithium sulfur (Li–S) couple stood out among various types of beyond Li-ion battery technologies due to high theoretical energy density (2600 Wh kg^{-1}), low toxicity, and worldwide abundance. Attributed to the appealing properties such as high theoretical capacity and low redox potential (−3.04 V vs. standard hydrogen electrode), lithium metal is the most ideal anode material for high energy density battery in both liquid electrolyte and solid state electrolytes (SSEs) configuration.[5,13,14] Nevertheless, one biggest concern of using lithium metal in battery is the notorious dendrite formation and associated safety risk. Derived from fractured solid electrolyte interface (SEI) and uneven lithium deposition, dendrite forms rapidly during initial cycles. As a consequence, the growing dendritic lithium is likely to penetrate the separator causing cell failure with short circuit and even detonation in the worst scenario.[15,16] Though the safety is expected to be improved by substituting SSEs for liquid electrolyte, the harmful dendrite formation/penetration still exists in most solid state batteries originated from the high electronic conductivity of SSE materials based on the most recent study.[17] Moreover, the poor compatibility of lithium with electrolyte would trigger side reactions on lithium metal-electrolyte interface forming electrochemically irreversible compounds, leading to low initial/cycling coulombic efficiency (CE) and poor cycling stability.[13,18]

One common strategy to address the above challenge is to create a stable SEI layer on top of lithium anode by introducing special electrolyte additives.[19–22] In this case, the protective layer is formed with the assistance of electrolyte additive in initial cycles preventing the continued decomposition of the electrolyte. However, this strategy often fails as the SEI layer is too brittle to fracture during cycling; i.e. it can hardly accommodate frequent volume change from lithium deposition/stripping resulting in the breakup of the layer and incubating more serious dendrite growth. An alternative strategy for dendrite suppression and lithium metal stabilization is to use specially designed SSE instead of the liquid electrolyte.[20,23–25] For example, Zhang group has recently developed an anion-immobilized poly(ethylene oxide)-$Li_{6.75}La_3Zr_{1.75}Ta_{0.25}O_{12}$ (PEO-LLZTO) composite electrolyte for

[a] *Dr. H. Zhong, Dr. Y. Zhao, Dr. G. Liu*
Energy Storage and Distributed Resources Division
Lawrence Berkeley National Laboratory
Berkeley, CA 94720, USA
E-mail: gliu@lbl.gov
[b] *Dr. H. Zhong*
Key Laboratory of Renewable Energy,
Guangdong Key Laboratory of Renewable Energy Research and Development,
Guangzhou Institute of Energy Conversion
Chinese Academy of Science
No.2 Nengyuan Rd., Guangzhou 510640, China
[c] *Dr. T. Zhang*
School of Automation
Beijing Institute of Technology
5 Zhongguancun St, Haidian District, Beijing 100811, China

[**] *Alq_3: Tris(8-hydroxyquinoline)aluminum*

Supporting information for this article is available on the WWW under https://doi.org/10.1002/batt.202000126

Special Collection *An invited contribution to a Special Collection on Lithium Metal Anode Processing and Interface Engineering*

dendrite free anode in all-solid-state battery.[25] Interestingly, Wang et al. reported realization of effective and robust Li passivation on Li/SSEs interface by introducing an intermediate layer of PEO/LiTFSI in their $Li_{1.5}Al_{0.5}Ge_{1.5}(PO_4)_3$-poly(ethylene oxide) solid-state battery.[23] However, most SSEs still suffer significantly from drawbacks such as low ionic conductivity, poor wetting effect, unstable lithium metal-SSE interface, and challenges on ultra-thin film manufacturing. Most recently, exciting progress has been made on developing non-SEI protective coatings for dendrite suppression and uniform lithium deposition. These include building porous layer to block direct contact between anode and electrolyte while allow precipitation of migrated Li^+ underneath the layer[16,26] or constructing layers with embedded selective seeds to intentionally induce Li deposition following a certain pattern.[27] The key of this strategy is to make sure a good electronic/ionic conductivity of those protective coatings for facile electron/ion transport during the charge/discharge process.

Copper current collector is widely used in the battery fabrication because of high conductivity and low cost. However, it is reported that lithium deposits randomly on Cu due to the poor affinity with Li, which leads to uncontrollable dendrite growth over long term cycling.[28] Therefore, copper substrate coated by aluminum thin film is often used for Li plating/stripping given that metallic Al has good lithiophilicity, high conductivity, and low materials cost. Upon initial contacting, lithium reacts with aluminum to form Li–Al alloy which provides lithiophilic sites for lithium nucleation and renders uniform deposition.[29,30] Nevertheless, capacity loss over cycles is still inevitable as the brittle metallic Al thin film can hardly remain intact in the process of alloying/dealloying. Herein, we propose a simple strategy to avoid aluminum fracture situation by using a tris-(8-hydroxyquinoline) aluminum (Alq_3) coated copper substrate. Alq_3 is a widely used organometallic compound which the centered Al^{3+} ion is coordinated with hydroxyquinoline ligands. Al^{3+} is expected to go through reduction to form atomic Al during the initial Li deposition. Given the unique chelate compound structure, Al is stabilized, protected, and separated by organic ligands in the smallest discrete unit, which could provide uniformly scattered lithophilic nucleation sites for lithium deposition, reduce the nucleation overpotential, and enhance structural integrity. Figure 1 demonstrates this idea schematically in comparison with the same lithium deposition process occurred on pure Cu and Al/Cu electrodes. Moreover, Alq_3 a conductive organometallic compound finds its application in light emitting diodes (LED) due to its high luminescence efficiency, excellent thermal stability, and low cost.[31,32] In addition to the promising usage of electron transportation and hole blockage, Alq_3 can be readily processed in the form of thin film by conventional techniques such as physical vapor deposition (PVD) or thermal evaporation, which makes it a perfect material for building non-SEI protective layer or substrate coating as discussed above.[33,34] In this work, key evaluation parameters such as coulombic efficiency, cycling stability, and polarization of various electrodes are investigated by Li plating/stripping test. Interface resistance of these electrodes is revealed by electrochemical impedance spectroscopy (EIS) measurement. Lithium deposition morphology characterized by SEM is compared as a function of differing conditions (coating thickness, current density etc.). Finally, the time evolution voltage curve as well as SEM images is used to study lithium dendrite growth on Cu, Al/Cu, Alq_3/Cu electrodes.

Results and Discussion

Molecular Structure and Properties of Alq_3

Alq_3 is a chelate compound with two common solvate polymorphs existed: α-Alq_3, β-Alq_3. Both phases have a triclinic crystal structure belonged to space group P-1.[35] As the molecular structure shown in Figure 2a, aluminum(III) was coordinated with three hydoxyquinoline ligands, forming a stable stereostructure through covalent bonds. This organometallic complex structure provides scattered metallic alumi-

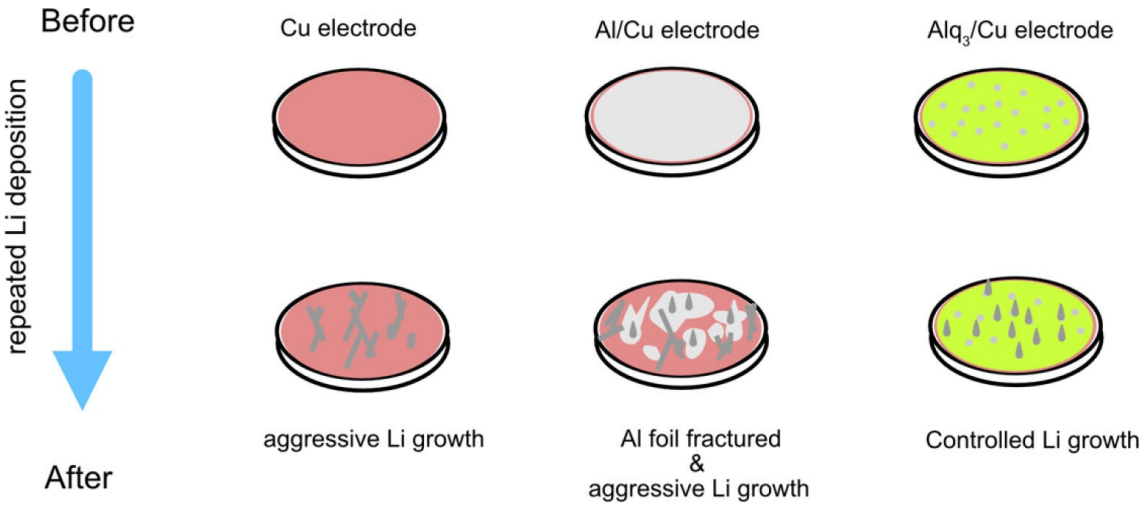

Figure 1. schematic diagram representing Li deposition process and dendrite growth as on different electrodes.

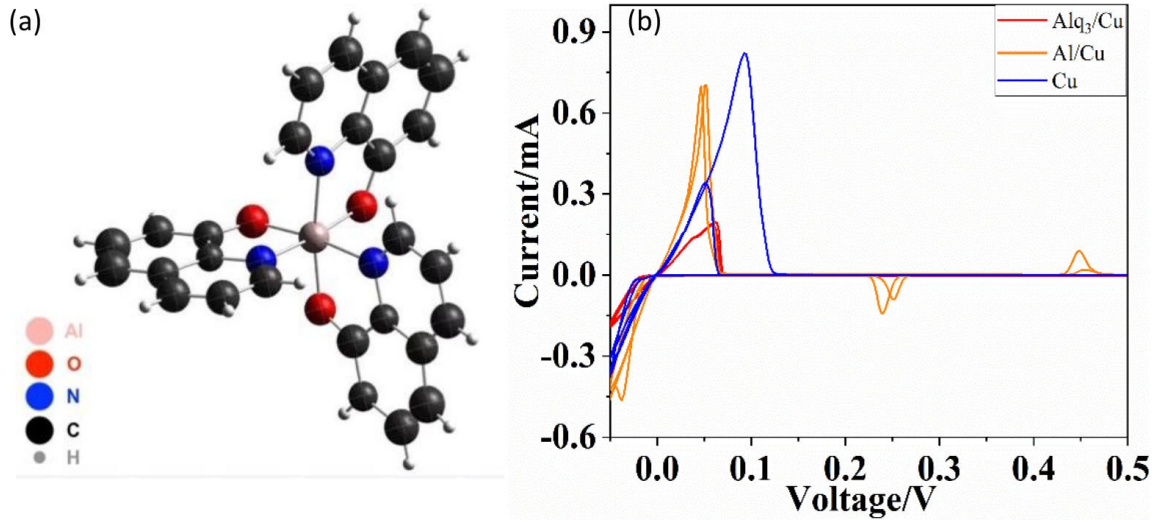

Figure 2. a) molecular structure of tris-(8-hydroxyquinoline) aluminum (Alq_3) chelate compound, b) cyclic voltammetry (CV) diagram of Alq_3/Cu, Al/Cu, and Cu electrodes in 1.0 M $LiPF_6$ in EC/DEC electrolyte with scanning electrochemical window of −0.05–0.5 V (vs. Li+/Li) and 0.02 mV/s scanning rate.

num units as Li nucleation sites and charge centers which is expected to induce more uniform lithium deposition. Cyclic voltammetry (CV) was conducted on Alq_3/Cu-50, Al/Cu (50 nm thickness) and pure Cu electrodes with the same sample size and the resulting diagrams were compared in Figure 2b. Redox peaks are observed at around 0 V (vs. Li/Li^+) for all three electrodes, representing lithium deposition ($Li+e^-\rightarrow Li$) and stripping ($Li\rightarrow Li^++e^-$) processes. The oxidation occurs at 0.05 V on both Alq_3/Cu and Al/Cu electrodes with good cycling consistency. In addition, the two coating samples exhibit smaller current intensity and integrated area, which indicates that less side reactions and improved electrochemical stability are enabled by Al-based coatings. Overall, Alq_3/Cu electrode exhibits the best CV performance among the three, demonstrating excellent stability and compatibility of Alq_3 for electrochemical applications such as Li plating/stripping. Admittedly, this benefit could be partially derived from the improved surface uniformity (Figure S1a and S1b). An extra oxidation and reduction peak are observed at approximately 0.5 V and 0.2 V on Al/Cu electrode due to the formation of Li–Al alloy (i.e., $Li^++e^-+Al\rightarrow LiAl$) and the corresponding dealloying process.[29] However, such alloying/dealloying behavior does not appear on Alq_3/Cu electrode suggesting aluminum element in Alq_3 thin film are non-metallic. This result agrees well with that aluminum exists discretely in Alq_3 compound at 3+ valence state, and is separated and stabilized by organic ligands. Thus, the structure integrity of thin film is largely enhanced by precluding alloy formation while the favorable lithiophilic sites is retained for lithium nucleation.

Li Plating/Stripping Test and Electrochemical Analysis

The Li plating/stripping test was performed to study both initial (ICE) and cycling coulombic efficiency (CE) as well as cycling stability on various Al-based coating electrodes and pure Cu electrode. Figure 3a and 3b displays the 1st cycle and the 300th cycle voltage profile of the plating/stripping test on pure Cu, Al/Cu (50 nm), and Alq_3/Cu-50, Alq_3/Cu-100 electrodes at a small current density of 0.05 mA cm^{-2}. At the initial cycle, Cu electrodes and both Alq_3/Cu electrodes exhibit normal potential behavior of plating/stripping process with comparably small polarization (~50 mV) suggesting the Alq_3/Cu has a good surface conductivity for facile charge transfer on par with the pure Cu electrode. While, the entire voltage curve of Al/Cu electrode shifted ~0.25 V up to the reference potential (0 V vs. Li/Li^+) at which the so-called Li–Al alloying/dealloying process took place. The ICE of those electrodes is pretty low because conditioning and electrolyte wetting process is always needed for the 1st cycle. At 300th cycle, all electrodes reveal improved CE and polarization due to the increasing surface area from repeated lithium stripping/deposition.[19] Among these, AlQ_3/Cu-50 electrode presents the highest CE (90.5%) and smallest polarization. It is worth noting that Al/Cu electrode does not show typical potential shift as usual Li–Al alloying/dealloying process does probably due to the fracture and peeling-off of Al coating over long cycles. The CE of plating/stripping test throughout 300 cycles on all electrodes were compared and displayed in Figure 3c. All exhibit CE retention in a reasonable range of 80–90% as is typical for carbonate based electrolyte,[19] while Alq_3/Cu-50 electrode outperforms others with the highest 91% CE on average because of high surface area and superior conductivity. This is then verified by electrochemical impedance spectroscopy (EIS) measurement which is usually used to examine interfacial resistivity of electrochemically active materials.[6,36] The Nyquist plot of all electrodes with 50% lithiation after 300 cycles are shown in Figure 3d. The interfacial resistivity increases with the coating thickness and the conductivity does not compromise much with the presence of organic ligands; the Alq_3 coating with 50 nm thickness exhibits small resistivity, nearly as comparable as that of metallic aluminum. Notably, the copper electrode is found to have a

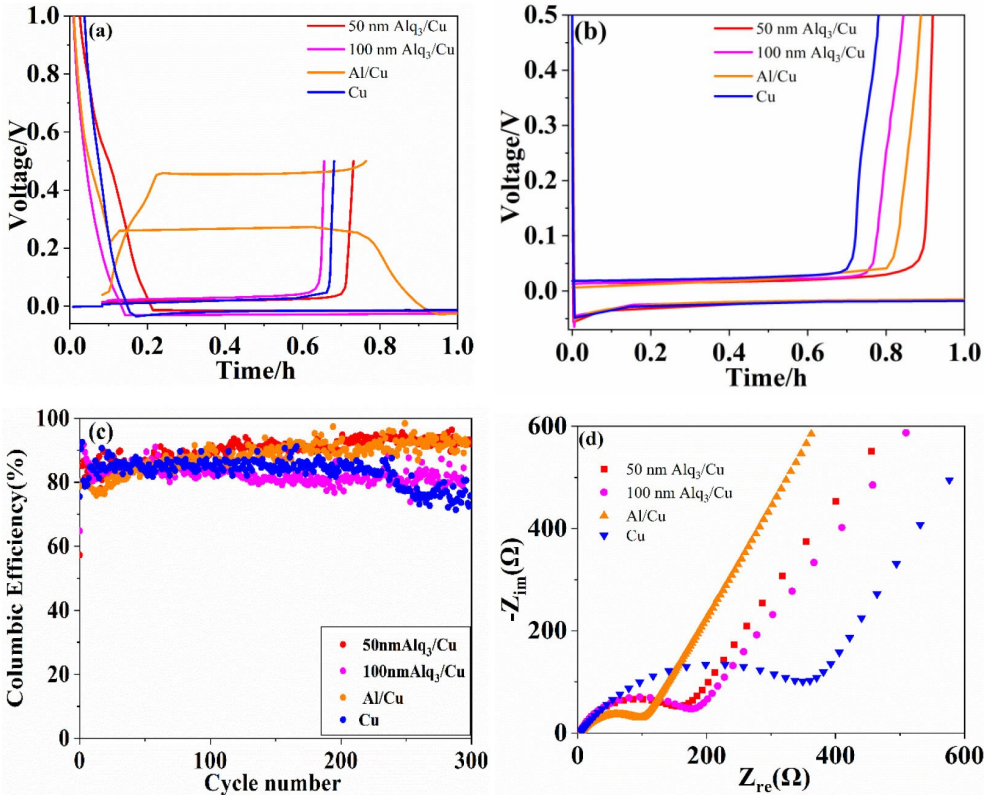

Figure 3. Li plating/stripping process at 0.05 mA/cm^2 current rate with 0.05 mAh/cm^2 deposition capacity as a function of substrates: a) Initial cycle voltage profile, b) 300th cycle voltage profile, c) CE over 300 cycles. d) EIS measurement with electrodes at 50% lithiation state after 300 cycles.

much large resistivity than expected which might be due to the inevitable oxidation layer on the surface.

Li Deposition Morphology

The fresh surface morphology of various Alq_3/Cu electrodes were characterized by SEM prior to Li plating/stripping as a function of coating thickness. Alq_3 compound was homogeneously deposited on the Cu current collector for all samples. However, some inhomogeneity like unsmooth edges are observed on the thin film of 50 nm and 100 nm sample. Figure S1d clearly shows that the copper substrate is covered by the coating material flawlessly at the thickness of 300 nm. Li plating was then performed on Alq_3/Cu-300 electrode as a function of deposition current density and time. After the plating cycle, the electrode was dissembled from the coin cell for SEM characterization to study deposition morphology (as shown in Figure S2). The rod-shaped lithium dendrites are formed and distributed evenly at low current density (I = 0.05 mA/cm^2) after 1 h deposition. With longer plating time (15 h deposition), rod dendrites start aggregating into a mossy chunk with significantly increased surface area. When current density increases to 0.1 mA/cm^2, dendrites remain the rod-like shape but with the formation of longer length; and again, a mossy chunk morphology was observed at 15 h deposition (Figure S2c and S2d). A nonuniform deposition occurs immediately after 6 min deposition when current density increases by one order of magnitude (Figure S3), suggesting a small current density is crucial for obtaining more orderly Li deposition.

Likewise, the Li plating test and corresponding SEM characterization were performed on Alq_3/Cu-50, Alq_3/Cu-100, and Alq_3/Cu-200 electrodes. Overall, flat depositing morphology suggests no aggressive growth of dendritic lithium on Alq_3/Cu-50 electrode at low current density (I = 0.05 mA/cm^2) (Figure 4a), which is in good agreement with the cell performance discussed above. However, rod-like micro dendrites with uniform distribution appears at higher current density (I = 1 mA/cm^2) (Figure 4b). For both Alq_3/Cu-100 and Alq_3/Cu-200 electrodes, the rod-like dendrites are present and uniformly distributed across the electrode surface at both low and high current density (Figure 4c–f). Unlike Alq_3/Cu-300 which is dominated by aggressive lithium dendrites growth, electrodes with 200 nm Alq_3 coating thickness or below render relatively orderly deposition and mild dendrite growth. As the control experiment, Li plating test was also performed on pure Li, pure Cu and Al/Cu electrodes under the same test conditions. The corresponding morphology for lithium deposition is revealed in Figure S4. In stark contrast with the result of Alq_3/Cu electrode, very poor deposition morphology is observed on those electrodes, which justifies Alq_3 coating protection would alleviate nonuniform lithium deposition and aggressive dendrite growth. In addition, those nodule-shape dendrites are formed in much

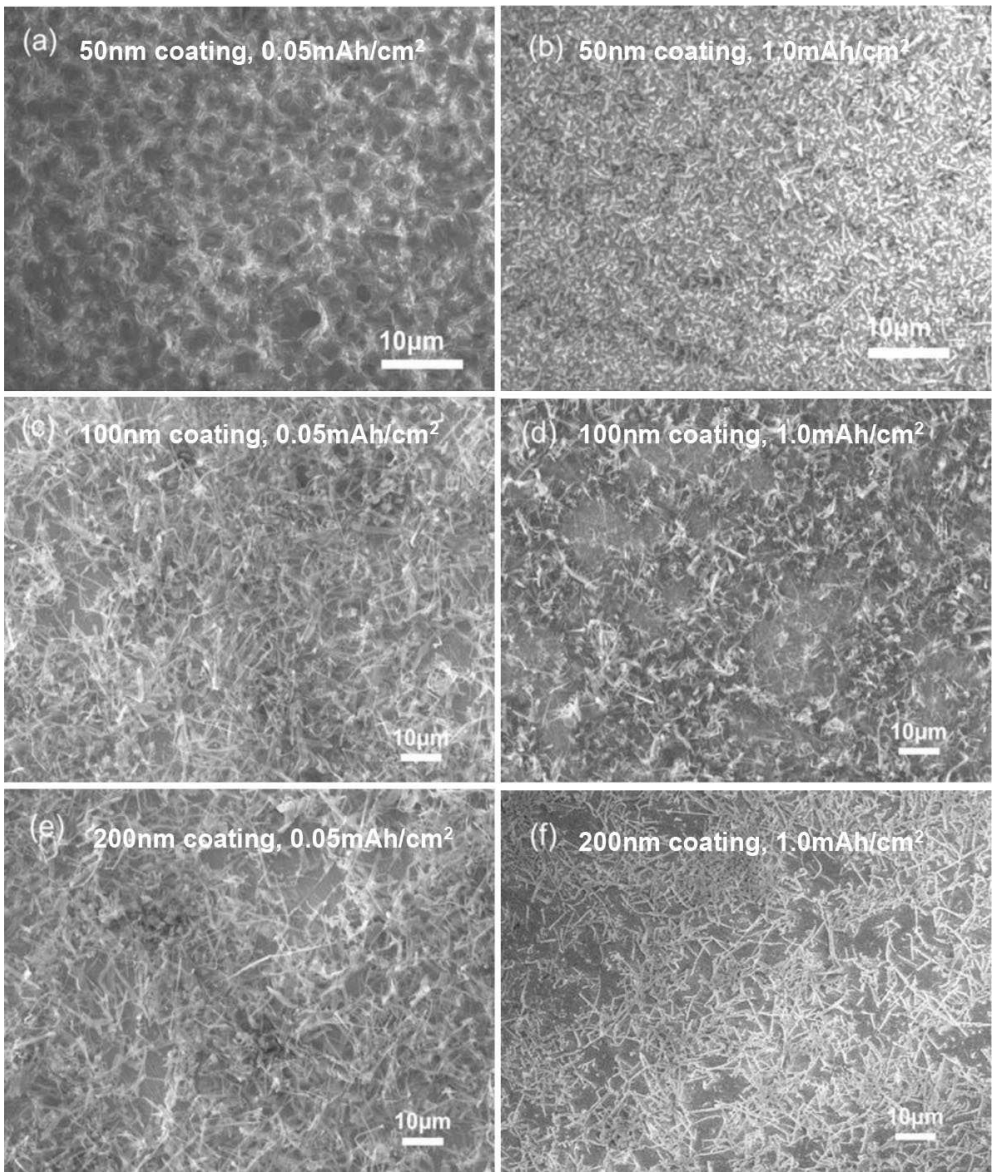

Figure 4. SEM of 1 h lithium deposition as a function of substrate and current density a) Alq_3/Cu-50, 0.05 mA/cm^2; b) Alq_3/Cu-50, 1 mA/cm^2; c) Alq_3/Cu-100, 0.05 mA/cm^2; d) Alq_3/Cu-100, 1 mA/cm^2; e) Alq_3/Cu-200, 0.05 mA/cm^2; f) Alq_3/Cu-200, 1 mA/cm^2.

bigger size, intertwined with one another and randomly distributed across the electrode surface.

Time Evolution Morphology Analysis on Lithium Deposition

The benefits of using Alq_3 substrate on lithium deposition and dendrites growth were further demonstrated by comparing time evolution morphology among Alq_3/Cu, pure Cu and Al/Cu electrodes. Lithium was first deposited on each target electrode by the time programmed, after which the electrode was dissembled from the cell for SEM morphology. The deposition voltage profile on electrodes are plotted with different color codes in Figure 5a. As you can tell, voltage curve is quite reproducible for each electrode which means a good consistency in the deposition process. As suggested by the potential profile of Alq_3/Cu electrodes, Al^{3+} goes through reduction to form atomic Al upon the initial Li deposition. The sloppy voltage drop at 0–0.33 h reflects this reduction process. The nucleation potential for Li deposition is 0.18 V, −0.045 V, and −0.025 V for Al electrode, Cu electrode, and Alq_3/Cu electrode respectively. The Li nucleation potential of Alq_3/Cu electrode is 0.02 V positive to that of Al/Cu electrode, indicating reduced nucleation overpotential was rendered by more dispersed and lithiophilic Al. Once again, the presence of a steady potential shift at 0.25 V on Al/Cu electrode indicates Li–Al alloy formation. Both Alq_3/Cu and pure Cu electrode demonstrate a typical potential diagram of lithium plating on non-alloying substrate. However, it takes about 8mins longer for Alq_3/Cu electrode to form the steady base potential, whereby the Al3+ is reduced and provide neucleation sites for lithium metal deposition. SEM morphology was checked on three electrodes

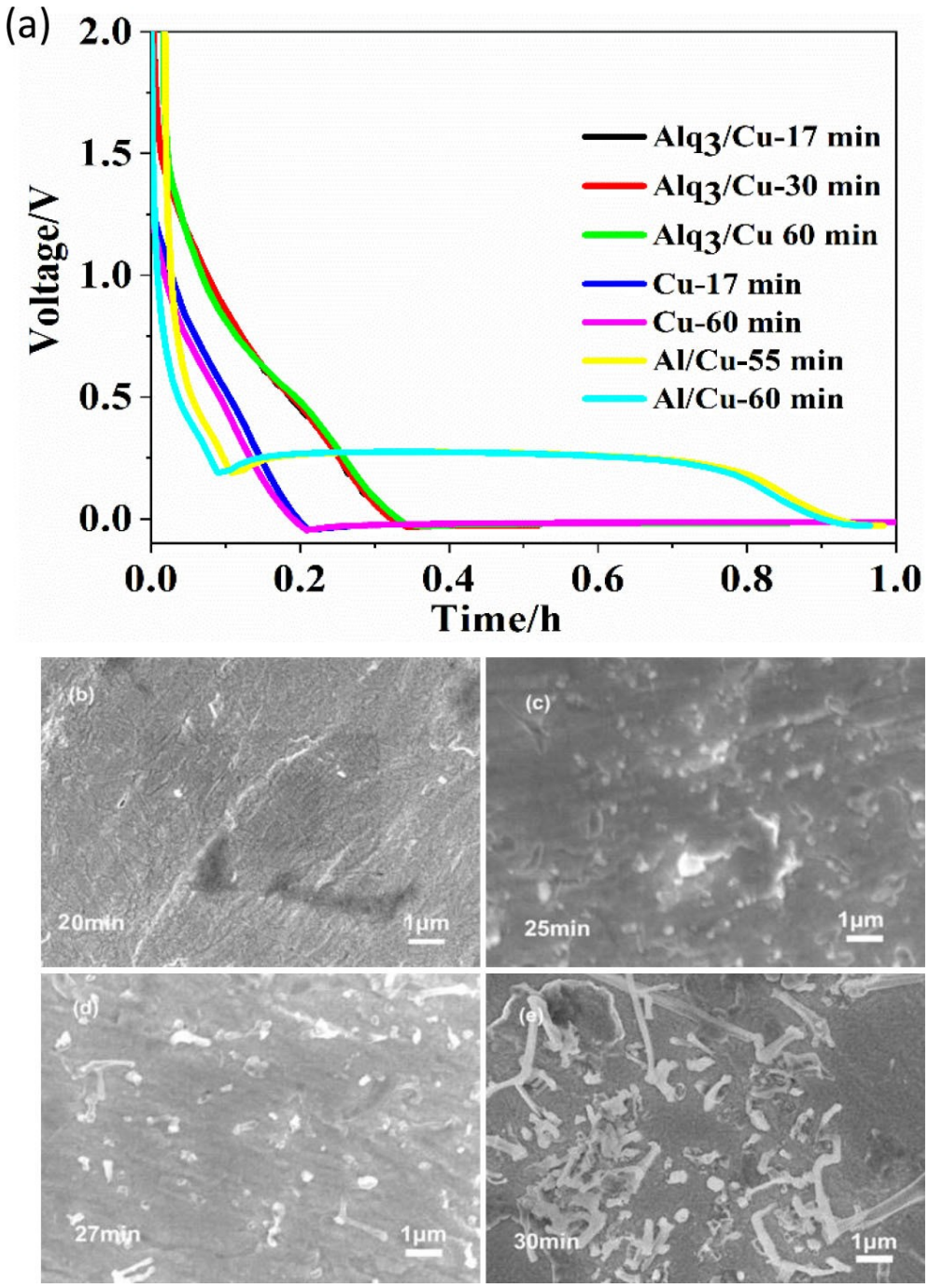

Figure 5. a) voltage profile for Li deposition at current density of 0.05 mA cm^{-2} as a function of substrates and deposition time. SEM morphology of Alq_3/Cu electrode surface at different Li deposition stages: b) 20th min, c) 25th min, d) 27th min, e) 30th min.

at different stages of the plating process. Figure 5b–e displays the morphology of Alq_3/Cu electrode at different stage of Li deposition (from 20 to 30 min, 0.05 mA cm^{-2} current density). Smooth surface morphology at the 20th mins suggests the process of reduction of the Al3+ and no lithium metal deposition. At 25th min, lithium nucleates uniformly across the film surface. From 27–30 min, lithium deposition grows into rod-shape as previously described. Similarly, the morphology change on Al/Cu and pure Cu electrodes is characterized and displayed in Figure S5. For pure Cu electrode, lithium dendrite shows up at the 17th min and thereafter aggressive growth is observed with the formation of thick nodule shape dendrites at the 60th min. While for Al/Cu electrode, it is clearly shown that a large portion of Al thin film looks fractured toward the end of 1 h deposition probably due to the volume expansion derived from the alloy formation.

Conclusions

In this work, we have reported a strategy to facilitate lithium deposition and prevent uncontrolled mossy dendrite growth by a conductive chelating compound Alq_3 as a surface modulation coating on copper current collector. Alq_3/Cu electrodes with various coating thickness were prepared through physical vapor deposition (PVD) method. The lithium plating/stripping tests were performed on those electrodes to study coulombic efficiency and dendrite formation at various current density. The performance difference was explained by the interface resistivity of various electrodes from results of electrochemical impedance spectroscopy measurement. The deposited lithium morphology on each electrode was systematically studied under different plating conditions. The improved CE performance and low interface resistance of Alq_3/Cu electrode with thickness <200 nm, as well as promising morphology results, validate the hypothesis that Alq_3 coating could provide discrete favorable lithiophilic sites for lithium nucleation and facilitate uniform distribution. This work has introduced a simple but effective strategy to render mild deposition and prevent uncontrolled and disordered lithium deposition and growth. This surface coating method can be integrated with other lithium dendrite prevention strategies to effectively address dendrite growth challenge for rechargeable lithium metal battery.

Experimental Section

Chemicals

Tris-(8-hydroxyquinoline) aluminum (Alq_3) and dimethyl carbonate (DMC, anhydrous, $\geq 99\%$) were ordered from Sigma-Aldrich. Li foil (thickness,178 μm) was purchased from FMC-Lithium Corp. Copper foil (thickness,16 μm) was bought from All-Foils Inc. Al foil (thickness, 20 μm) was purchased from Furukawa Electric Corp. LTD. The electrolyte 1.0 M lithium hexafluorophosphate ($LiPF_6$) in ethylene carbonate (EC, 99%)/diethylene carbonate (DEC, 99%) (H_2O content <10 ppm) were purchased from BASF Chemical Company. All chemicals were used as received without further purification.

Electrodes Fabrication and SEM Characterization

Alq_3 was coated on copper foil through physical vapor deposition (PVD). The process was operated in the vacuum chamber under the pressure of 10^{-4} Pa, at the current rate of 1 A/s. The as-obtained Alq_3/Cu film was synthesized and dried at 60 °C in a vacuum oven for 12 h. For the sake of simplification, the Alq_3/Cu sample electrodes with thickness of 50, 100, 200, and 300 nm are denoted as Alq_3/Cu-50, Alq_3/Cu-100, Alq_3/Cu-200, and Alq_3/Cu-300, respectively. The control sample Al thin film coated Cu, denoted as Al/Cu, with the thickness of 50 nm was prepared in the same way from PVD method. Surface morphology of the electrode post plating test is characterized by a JEOL JSM-7500F field emission scanning electron microscope with an accelerating voltage of 10 kV using the high vacuum mode at room temperature. All electrode samples were assembled into coin cells in the glovebox (Vacuum Technology Inc., <0.5 ppm O_2 and H_2O) where the electrode disk was also dissembled and then mounted on a stub specimen by carbon tape for SEM characterization after electrochemical tests. The sample was placed in the Ar-filled container during the transfer and was exposed to the air less than 5 s before finally loaded into SEM instrument. The electrodes were carefully washed by diethylene carbonate (DEC) to get rid of any impurity residual from the cell prior to postmortem analysis.

Electrochemical Performance Measurement

Li||Cu cell was assembled in coin cells (CR2325, National Research Council Canada) for Li plating/stripping test. Circular copper discs were punched with an area of 1.6 cm^2 and were assembled on the cathode side. Lithium foil (thickness, 178 μm) was employed as the anode with an area of 1.88 cm^2 attached onto a stainless steel spacer. The cell assembly was performed in an Ar-filled glove-box using 1 M $LiPF_6$ EC/DEC (v/v = 1/1) as the electrolyte, and polypropylene separator (Celgard 2400). Likewise, Li||(Al/Cu), and Li||(Alq_3/Cu) cells were also fabricated. Galvanostatic lithium plating/stripping test was then performed on sample cells Li||Cu, Li||(Al/Cu), and Li||(Alq_3/Cu) using Maccor battery cycler. All cells were placed in the isothermal oven and tested under ambient temperature at various current densities (0.05 mA cm^{-2}, 0.1 mA cm^{-2}, and 1 mA cm^{-2}) with the voltage range of -0.05 to 0.5 V vs. Li^+/Li. The areal deposition capacity for this process was 0.08 mAh/cm^{-2}. Cyclic voltammetry (CV) was carried out on a potentiostat (Bio-Logic SAS, France) to study electrochemical stability of the electrode with the voltage window of -0.05 to 0.5 V (vs. Li^+/Li) and a scanning rate of 0.02 mV s^{-1}. Electrochemical impedance spectroscopy (EIS) measurements (Autolab, Metrohm) were conducted on Alq_3/Cu, Al/Cu and pure Cu foil electrodes with 50% lithiation after the 300th cycle in the frequency range of 0.001 Hz to 1 MHz.

Acknowledgements

This work was funded by the Assistant Secretary for Energy Efficiency, Vehicle Technologies Office of the U.S. Department of Energy, under the Advanced Battery Materials Research (BMR) Program. Lawrence Berkeley National Laboratory (LBNL) is supported by the Director, Office of Science, Office of Basic Energy Sciences, of the US Department of Energy under contract no. DE-AC02-05CH11231.

Conflict of Interest

The authors declare no conflict of interest.

Keywords: lithium metal anode · Alq_3 conductive compound · conductive coating · controlled Li deposition · coulombic efficiency

[1] X. Fan, L. Chen, O. Borodin, X. Ji, J. Chen, S. Hou, T. Deng, J. Zheng, C. Yang, S. C. Liou, K. Amine, K. Xu, C. Wang, *Nat. Nanotechnol.* **2018**, *13*, 715–722.
[2] B. Dunn, H. Kamath, J. M. Tarascon, *Science* **2011**, *334*, 928–935.
[3] K. Hietala, Y. Zhao, Y. Yang, C. A. Wolden, *Ind. Eng. Chem. Res.* **2018**, *57*, 8436–8442.
[4] X. Li, Y. Zhao, A. Brennan, M. McCeig, C. A. Wolden, Y. Yang, *ChemSusChem* **2017**, *10*, 2904–2913.

[5] Y. Zhao, W. Smith, C. A. Wolden, *J. Electrochem. Soc.* **2020**, *167*.
[6] Y. Zhao, Y. Yang, C. A. Wolden, *ACS Appl. Energy Mater.* **2019**, *2*, 2246–2254.
[7] C. P. Grey, J. M. Tarascon, *Nat. Mater.* **2016**, *16*, 45–56.
[8] P. G. Bruce, S. A. Freunberger, L. J. Hardwick, J. M. Tarascon, *Nat. Mater.* **2011**, *11*, 19–29.
[9] Y. Zhao, C. Fang, G. Zhang, D. Hubble, A. Nallapaneni, C. Zhu, Z. Zhao, Z. Liu, J. Lau, Y. Fu, G. Liu, *Front. Chem.* **2020**, *8*.
[10] R. Xu, X.-B. Cheng, C. Yan, X.-Q. Zhang, Y. Xiao, C.-Z. Zhao, J.-Q. Huang, Q. Zhang, *Matter.* **2019**, *1*, 317–344.
[11] R. Xu, Y. Xiao, R. Zhang, X. B. Cheng, C. Z. Zhao, X. Q. Zhang, C. Yan, Q. Zhang, J. Q. Huang, *Adv. Mater.* **2019**, *31*, e1808392.
[12] Z. Liu, X. He, C. Fang, L. E. Camacho-Forero, Y. Zhao, Y. Fu, J. Feng, R. Kostecki, P. B. Balbuena, J. Zhang, J. Lei, G. Liu, *Adv. Funct. Mater.* **2020**.
[13] Y. Guo, H. Li, T. Zhai, *Adv. Mater.* **2017**, *29*.
[14] X. B. Cheng, R. Zhang, C. Z. Zhao, F. Wei, J. G. Zhang, Q. Zhang, *Adv. Sci. (Weinh).* **2016**, *3*, 1500213.
[15] D. Wang, W. Zhang, W. Zheng, X. Cui, T. Rojo, Q. Zhang, *Adv. Sci (Weinh).* **2017**, *4*, 1600168.
[16] G. A. Umeda, E. Menke, M. Richard, K. L. Stamm, F. Wudl, B. Dunn, *J. Mater. Chem.* **2011**, *21*, 1593–1599.
[17] F. Han, A. S. Westover, J. Yue, X. Fan, F. Wang, M. Chi, D. N. Leonard, N. J. Dudney, H. Wang, C. Wang, *Nat. Energy* **2019**, *4*, 187–196.
[18] J. Zheng, J. A. Lochala, A. Kwok, Z. D. Deng, J. Xiao, *Adv. Sci. (Weinh).* **2017**, *4*, 1700032.
[19] H. Wu, Y. Cao, L. Geng, C. Wang, *Chem. Mater.* **2017**, *29*, 3572–3579.
[20] Y. Liu, D. Lin, Y. Li, G. Chen, A. Pei, O. Nix, Y. Li, Y. Cui, *Nat. Commun.* **2018**, *9*, 3656.
[21] H. Zhang, G. G. Eshetu, X. Judez, C. Li, L. M. Rodriguez-Martinez, M. Armand, *Angew. Chem. Int. Ed.* **2018**, *57*, 15002–15027.
[22] W. Li, H. Yao, K. Yan, G. Zheng, Z. Liang, Y. M. Chiang, Y. Cui, *Nat. Commun.* **2015**, *6*, 7436.
[23] C. Wang, Y. Yang, X. Liu, H. Zhong, H. Xu, Z. Xu, H. Shao, F. Ding, *ACS Appl. Mater. Interfaces* **2017**, *9*, 13694–13702.
[24] B. Xu, W. Li, H. Duan, H. Wang, Y. Guo, H. Li, H. Liu, *J. Power Sources.* **2017**, *354*, 68–73.
[25] C. Z. Zhao, X. Q. Zhang, X. B. Cheng, R. Zhang, R. Xu, P. Y. Chen, H. J. Peng, J. Q. Huang, Q. Zhang, *Proc. Natl. Acad. Sci. USA* **2017**, *114*, 11069–11074.
[26] J. Bobnar, M. Lozinsek, G. Kapun, C. Njel, R. Dedryvere, B. Genorio, R. Dominko, *Sci. Rep.* **2018**, *8*, 5819.
[27] K. Yan, Z. Lu, H.-W. Lee, F. Xiong, P.-C. Hsu, Y. Li, J. Zhao, S. Chu, Y. Cui, *Nat. Energy* **2016**, *1*.
[28] H. Ye, Z. J. Zheng, H. R. Yao, S. C. Liu, T. T. Zuo, X. W. Wu, Y. X. Yin, N. W. Li, J. J. Gu, F. F. Cao, Y. G. Guo, *Angew. Chem. Int. Ed.* **2019**, *58*, 1094–1099.
[29] A. S. Baranski, W. R. Fawcett, *J. Electrochem. Soc.* **1982**, *129*, 901–907.
[30] Y. Hamon, T. Brousse, F. Jousse, P. Topart, P. Buvat, D. M. Schleich, *J. Power Sources* **2001**, *97*, 185–187.
[31] N. Johansson, T. Osada, S. Stafström, W. R. Salaneck, V. Parente, D. A. dos Santos, X. Crispin, J. L. Brédas, *J. Chem. Phys.* **1999**, *111*, 2157–2163.
[32] A. Zawadzka, P. Płóciennik, J. Strzelecki, Z. Łukasiak, B. Sahraoui, *Opt. Mater.* **2013**, *36*, 91–97.
[33] J. S. Jung, J. W. Lee, M. R. Seo, H. S. Lee, J. Kim, S. W. Lee, J. Joo, *Synth. Met.* **2012**, *162*, 1852–1857.
[34] W. Xie, W. W. He, D. Y. Du, S. L. Li, J. S. Qin, Z. M. Su, C. Y. Sun, Y. Q. Lan, *Chem. Commun. (Camb.)* **2016**, *52*, 3288–3291.
[35] M. Brinkmann, G. Gadret, M. Muccini, C. Taliani, N. Masciocchi, A. Sironi, *J. Am. Chem. Soc.* **2000**, *122*, 5147–5157.
[36] C. M. A. B. Brett, A. M. O., *Bringing materials to book. Electrochemistry-principles, methods and applications*, Oxford University Press, **1993**.

Manuscript received: June 2, 2020
Revised manuscript received: July 23, 2020
Accepted manuscript online: August 3, 2020
Version of record online: September 7, 2020